



Development of waste brine to energy system with Concentric Cylindrical Thermoelectric Generator (CCTEG) at Ulubelu Geothermal Power Plant

Mochammad Resha¹, Tubagus Ahmad Fauzi Soelaiman², Hendi Riyanto³, Parman Parman⁴

¹Jurusan Teknik Mesin, Fakultas Teknik, Universitas Lampung

²Jurusan Teknik Mesin, Fakultas Teknik Mesin Dirgantara, Institut Teknologi Bandung

³Jurusan Teknik Mesin, Fakultas Teknik Mesin Dirgantara, Institut Teknologi Bandung

⁴Jurusan Teknik Bangunan Kapal Politeknik Perkapalan Negeri Surabaya. Kampus ITS Keputih Sukolilo

email: m.resha@eng.unila.ac.id

Info Artikel :

Diterima :

21 Januari 2025

Disetujui :

10 Februari 2025

Dipublikasikan :

25 Februari 2025

ABSTRACT

The Ulubelu geothermal field plan to utilize geothermal energy through the direct use energy of brine. Develop waste to energy a Thermoelectric Generator (TEG) into the system represents an innovative approach to harness additional energy from the high-temperature brine before it is reinjected into the well. The Circular Construction Thermoelectric Generator (CCTEG) is designed using a double-pipe heat exchanger, with diameters of 1.02 m for the brine and 0.91 m for the cold water. The brine enters at 174°C with a mass flow rate of 763 kg/s, while the condensate water from the cooling tower is at 28°C. Simulation results show that the CCTEG requires 2309370 TEG semiconductors along a 32-meter length, achieving a power output of 538.25 kW with a total voltage of 51.2 kV and a current of 10.5 A. The system experiences pressure drops of 189 kPa on the hot side and 1,869 kPa on the cold side, utilizing 0.6% of the total brine energy potential of 79760 kW. This design demonstrates an efficient method to optimize energy extraction from geothermal resources.

Keywords : Brine, Energy extraction, Geothermal energy, Circular Construction Thermoelectric Generator (CCTEG)



©2022 Penulis. Diterbitkan oleh Arka Institute. Ini adalah artikel akses terbuka di bawah lisensi Creative Commons Attribution NonCommercial 4.0 International License. (<https://creativecommons.org/licenses/by-nc/4.0/>)

INTRODUCTION

The increase in the global population over the past decade, makes energy demand expected to increase International Energy Agency (IEA) projections, Global electricity demand is forecast to grow by around 4% in 2024, up from 2.5% in 2023. This would represent the highest annual growth rate since 2007, excluding the exceptional rebounds seen in the wake of the global financial crisis and the Covid-19 pandemic. The strong increase in global electricity consumption is set to continue into 2025, with growth around 4% again, according to the report (IEA Report, 2024) The growth of renewable energy generation, such as wind and solar power in this decade is quite significant. However, to fully meet the two conflicting requirements of higher energy demand and reduced CO₂ emissions, it is also important to achieve maximum efficiency of the energy used. Low-grade waste heat alone accounts for at least 50% of the total heat generated in industry and has been proven to represent 9.5% of all industrial energy consumption in the world. Nationally Determined Contributions (NDCs), long-term low greenhouse gas emission development strategies (LT-LEDS) and net-zero targets, if fully implemented, could reduce reduced CO₂ emissions by 6% by 2030 and 56% by 2050, compared to 2022 levels (IRENA, 2023)

In conventional power generation systems, about half of the resources are wasted as a result of limited power conversion. Waste heat recovery, therefore, provides economic and environmental benefits as it drives greater overall efficiency, which in turn leads to lower demand for resources required for power generation and lower CO₂ emissions. The Ulubelu Geothermal Power Plant has a potential exergy rate of 48025 kW in the form of brine (steam or liquid) which is injected back into the well (Mughtar et al., 2018). Carrying the concept of waste to energy, geothermal brine should be able to be used for Thermoelectric Generators (TEG) as additional power plants. TEG as a semiconductor device that generates electricity from two temperature differences on both surfaces based on the Seebeck effect (Madruga, 2021). Thermoelectric generators (TEGs) appear to be a good choice for

generating heat from waste heat. Thermoelectric generators are devices working principally by Seebeck effect which can convert heat directly to electricity (Al-Habahbeh et al., 2018). Since they have a straightforward structure with no moving parts, they are very convenient for small-scale applications. Moreover, they have a very low maintenance cost, no operation cost, and no emission of greenhouse gas emissions. The annular thermoelectric module called the Concentric Circular Thermoelectric Generator (CCTEG) is a TEG model that is being further developed because it has several advantages such as being able to load more thermoelectric modules and having less contact resistance than the flat plate TEG model (Bauknecht et al., 2013). The use of CCTEG is suitable for use in heat dissipation pipelines such as motor vehicle exhaust or geothermal fluid reinjection pipes that still have energy potential to be utilized.

Several studies by (T. Ding et al., 2020) made mathematical modeling on CCTEG which has 1500 x 470 P-N pairs of semiconductors in 100 segments along 500 m. Analysis using Engineering Equation Solver (EES) at a temperature difference of 130°C produces a CCTEG power of 136 kW arranged in series. (L. C. Ding et al., 2015) conducted a study on the utilization of geothermal fluids using thermoelectric cells (TECs) on a circular heat exchanger with a capacity of 1800 kW. The results of the analysis require TECs of 350000 to 520000 or equivalent to a heat exchanger 350 m to 520 m long. The large-scale utilization of TEG technology can play an important role in shaping the power generation industry from thermal energy, including from solar, geothermal, biomass, industrial waste heat, and others. TEG has not been widely marketed due to higher costs and low efficiency. The cost of a heat exchanger usually dominates the cost of the TEG system as a whole. To get a TEG system cost of \$1/W, a heat exchanger fee of \$1/(W/°C) is required (Li et al., 2021).

Ulubelu Geothermal Power Plant has the potential for direct utilization of geothermal energy utilizing brine with the development of Concentric Circular Thermoelectric Generator energy conversion technology. The development of this energy conversion technology is carried out by calculating the potential energy of brine based on the silica saturation level using SSI parameters. The design of the CCTEG was carried out by analyzing the heat transfer of each segment in a volume control manner. The CCTEG power produced is influenced by the characteristics of the materials that make up TEG semiconductors, namely Seebeck Coefficient, Electrical Resistivity, and Thermal Conductivity. In addition to generating additional power, the cold water that comes out of the CCTEG can be used for various utility needs such as hot springs with a temperature of around 40°C. Reusing wasted energy is becoming a viable option, particularly for energy-intensive industries whose production processes discharge significant amounts of heat into the environment, typically air or water. (Zoui et al., 2022)

The study will design CCTEG to generate electrolysis system for hydrogen production. CCTEG is designed to utilize brine from separation of the three separators and cold fluid using condensate water from the cooling towers to condensate pool. In this study using the Hi-Z Technology brand TEG module with Bismuth Telluride (Bi-Te) material. The design of CCTEG was carried out by calculating the brine potential according to the Sillica Saturation Index. CCTEG is composed of TEG semiconductors that adjust the conditions inside a concentric circular heat exchanger. The design results in technical parameters such as the length of the TEG, number of semiconductors, thermal conditions, and output power of the CCTEG.

RESEARCH METHODS

This study is a basic design study CCTEG at Ulubelu Geothermal Power Plant, Indonesia to utilize of different temperatures from brine and water condensate. Research scheme as seen in Figure 1

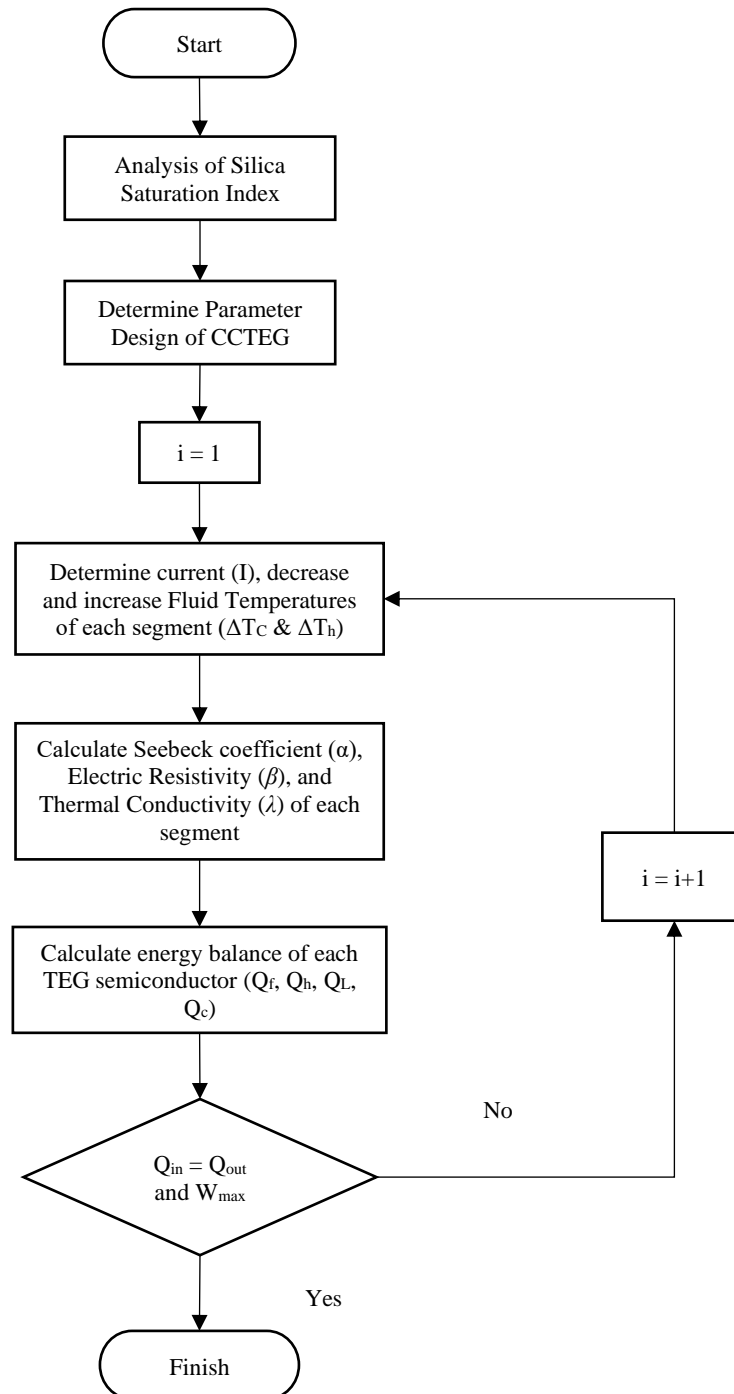


Figure 1. Research Schematic

The characteristics of brine in the Ulubelu Geothermal Field in this study have a temperature, pressure, mass rate, and silica content, shown in Table 1.

Table 1. Brine content

Parameter	Symbol	Value	Unit
Temperature	T	174	$^{\circ}\text{C}$
Pressure	P	0.869	MPa
Mass flow	\dot{m}	763.73	kg/s
Silica Content	S	599	ppm

Harvesting the energy from the use of brine, the silica deposition factor occurs when the temperature is lower than the temperature of the reservoir. Silica deposition can occur on the surface of pipes, separators, scrubbers, heat exchangers including TEG. In geothermal reservoirs, there is an equilibrium of silica in the form of quartz according to the following reaction, shown in equation 1. (DiPippo, 2015).



When the silica concentration in the brine is higher than the silica saturation concentration calculated at a certain temperature, the amorphous silica will begin to precipitate. The reaction is dependent on temperature, pH, and salinity. The saturation level of silica is determined through the silica saturation index (SSI) value shown in equation 2

$$SSI = \frac{s}{s_{sat}} \quad (2)$$

The solubility of amorphous *silica* in water affected by temperature and salinity shown in equation 3 (DiPippo, 2015)

$$S_{sat} = s \cdot 10^{-mD(t)} \quad (3)$$

Some variables are described by Equation 3 (DiPippo, 2015)

$$\text{Log } s = 4,52 - \frac{751}{T} \quad (4)$$

$$\text{Log } D(t) = -1,0596 - 0,001573 \cdot T \quad (5)$$

$$m = \frac{CL}{35,5 \cdot 1000} \quad (6)$$

SSI parameters were used to estimate silica scaling conditions, with the following criteria SSI > 1, and fluids in supersaturated conditions, silica deposition is possible.) SSI = 1, fluid in a saturated condition. SSI < 1, the fluid is unsaturated, so silica deposition is not possible (DiPippo, 1985). Binary cycle power plants have a value of SSI = 1.5 as the limit of silica deposition (DiPippo, 2015). The brine content in the Ulubelu geothermal field has an acidity level (PH) of around 6 – 8 with a chemical composition of Silica of 599 ppm (Darmawi & Malau, 2018).

The components of TEG are semiconductors that are arranged in parallel or series. The performance of semiconductors is influenced by the type of material used. In this study, the TEG module of the Hi-Z Technology brand was used with Bismuth Telluride (Bi-Te) material. The arrangement of TEG element components is shown in Figure 2 (Hi-Z, 2017).

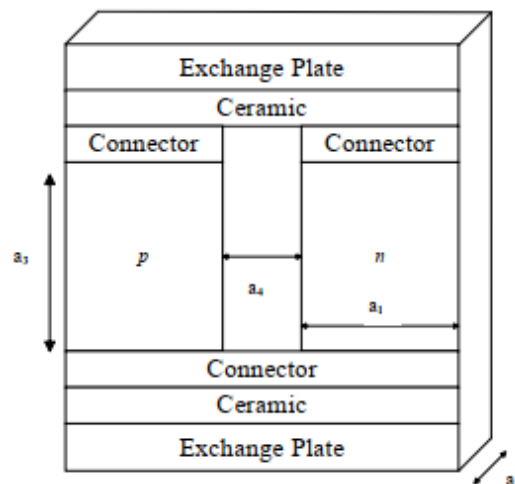


Figure 2. Components of TEG Semiconductor

Specification of TEG semiconductor for each component shown in Table 2 (Hi-Z, 2017).

Table 2. Specification of TEG Semiconductor

Parameter	Length	Unit
$a_1 = a_2$	0.0058	m
a_3	0.0025	m
a_4	0.0001	m
$\delta_{\text{ex. plate}}$	0.002	m
δ_{ceramic}	0.001	m
$\delta_{\text{connector}}$	0.001	m
$\lambda_{\text{ex. plate}}$	398	W/m.k
$\lambda_{\text{connector}}$	398	W/mk.
λ_{ceramic}	35	W/mk.

Several TEG parameters such as Seebeck coefficient (α), electrical resistivity (β), and thermal conductivity (λ) always change according to the average temperature of each segment (He et al., 2020).

$$\alpha_p(\bar{T}) = \frac{161 - 1,818\bar{T} + 0,01113\bar{T}^2 - 2,035 \cdot 10^{-5}\bar{T}^3 + 1,134 \cdot 10^{-8}\bar{T}^4}{10^6} \quad (7)$$

$$\alpha_n(\bar{T}) = \frac{-442,8 + 3,469\bar{T} + 0,0142\bar{T}^2 - 2,325 \cdot 10^{-5}\bar{T}^3 + 1,3 \cdot 10^{-8}\bar{T}^4}{10^6} \quad (8)$$

$$\beta_p(\bar{T}) = \frac{-5,01 + 0,03519\bar{T} + 7,74 \cdot 10^{-5}\bar{T}^2 - 8,94 \cdot 10^{-9}\bar{T}^3 + 4,32 \cdot 10^{-12}\bar{T}^4}{10^5} \quad (9)$$

$$\beta_n(\bar{T}) = \frac{-0,8072 + 0,004507\bar{T} + 7,827 \cdot 10^{-6}\bar{T}^2 - 8,94 \cdot 10^{-8}\bar{T}^3 + 1,317 \cdot 10^{-12}\bar{T}^4}{10^5} \quad (10)$$

$$\lambda_p(\bar{T}) = \frac{-469,7 + 4,57\bar{T} - 0,01575\bar{T}^2 + 2,331 \cdot 10^{-5}\bar{T}^3 - 1,242 \cdot 10^{-8}\bar{T}^4}{10} \quad (11)$$

$$\lambda_n(\bar{T}) = \frac{101,2 - 0,7414\bar{T} - 0,002246\bar{T}^2 - 3,019 \cdot 10^{-6}\bar{T}^3 + 1,537 \cdot 10^{-9}\bar{T}^4}{10} \quad (12)$$

Figure 3 shown the design of a Concentric Circular Thermoelectric Generator (CCTEG) integrated within a heat exchanger system. The configuration employs a counterflow arrangement with two primary circuits for hot and cold fluids, complemented by embedded CCTEG modules that convert thermal gradients into electrical energy through the thermoelectric effect. Secondary circuits containing brine provide auxiliary heat transfer capacity, enhancing the system's thermal management. This innovative adaptation of a shell-and-tube heat exchanger architecture strategically positions CCTEG components to simultaneously optimize both thermal exchange efficiency and electrical power generation. The concentric design enables efficient thermal energy recovery while maintaining compact system dimensions, making it particularly suitable for applications requiring combined heat transfer and energy harvesting capabilities.

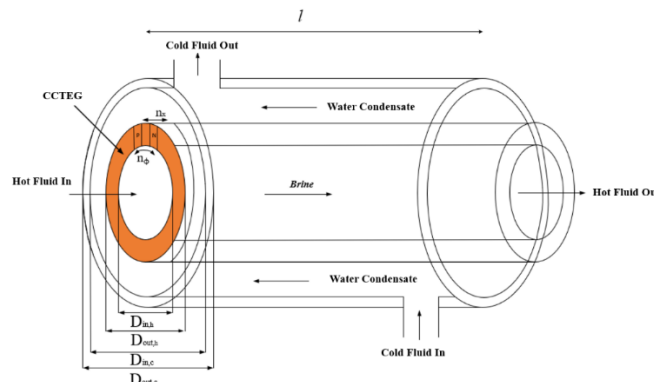


Figure 3. Modeling of Heat Exchanger with CCTEG

Table 3. Design of Heat Exchanger with CCTEG

Parameter	Length	Unit
$D_{\text{out,h}}$	0,914	m
$D_{\text{in,h}}$	0,905	m
$D_{\text{out,c}}$	1,016	m

Parameter	Length	Unit
$D_{in.c}$	1,007	m
n_{ϕ}	490	
Δ_x	0,0068	m

Heat transfer in the components of the TEG element is affected by the value of Seebeck's coefficient, electrical resistance, and thermal conductivity to find the temperature value of each segment and the electrical power generated shown in Equation 13 – 15 each on P-N Junction segment (Yang et al., 2022)

$$\alpha_{pn} = \alpha_{pn} - \alpha_n \quad (13)$$

$$\beta_{pn} = D_{in.h} \cdot \ln \left[\frac{(D_{in.h} + a_3)}{D_{in.h}} \right] \cdot (\beta_p + \beta_n) / (a_1 \cdot a_2) \quad (14)$$

$$\lambda_{pn} = a_1 \cdot a_2 \cdot (\lambda_p + \lambda_n) / \left(D_{in.h} \ln \left[\frac{D_{in.h} + a_3}{D_{in.h}} \right] \right) \quad (15)$$

Schematic of energy balance on a TEG semiconductor is shown in Figure 4.

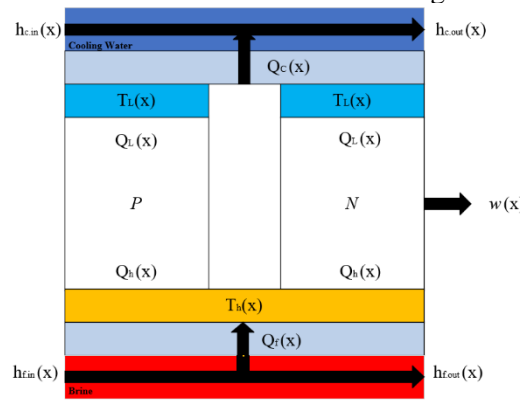


Figure 4. Schematic of TEG energy balanced

Energy balance of the TEG segment is shown at Equation 16 and 17.

$$\dot{Q}_f = \dot{Q}_h \quad (16)$$

$$\dot{Q}_L = \dot{Q}_c \quad (17)$$

The hot side of the heat released from the brine to each TEG segment, there is a transfer of convection heat to the surface of the CCTEG and the cold side of the water receives heat from the surface of the CCTEG shown in Equations 18 and 19.

$$\dot{Q}_f(x) = h_{f.out}(x) - h_{f.in}(x) = n_{\phi} \cdot h_f \cdot A \cdot \left[\frac{T_{fh}(x) + T_{fh}(x+dx)}{2} - T_h(x) \right] \quad (18)$$

$$\dot{Q}_c(x) = h_{c.out}(x) - h_{c.in}(x) = n_{\phi} \cdot h_c \cdot A \cdot \left[T_L(x) - \frac{T_{fh}(x) + T_{fh}(x+dx)}{2} - T_h(x) \right] \quad (19)$$

Equations 20 and 21 show the heat absorbed on the hot side and cold side of CCTEG being converted into electrical energy in each segment.

$$\dot{Q}_h(x) = n_{\phi} \left[\alpha \cdot I \cdot T_h(x) + \beta_{pn}(T_h(x) - T_L(x)) - \frac{1}{2} \cdot I^2 \cdot \beta_{pn} \right] \quad (20)$$

$$\dot{Q}_L(x) = n_{\phi} \left[\alpha \cdot I \cdot T_L(x) + \beta_{pn}(T_h(x) - T_L(x)) + \frac{1}{2} \cdot I^2 \cdot \beta_{pn} \right] \quad (21)$$

Convection Coefficient in each segment on the hot and cold side to be calculated based on equation at Table 4.

Table 4. Equation of Convection Coefficient

Parameter	Hot side	Cold Side	Unit
h	$Nu(x) \cdot \frac{k}{D_{in,h}}$	$Nu(x) \cdot \frac{k}{D_{in,h} - D_{in,c}}$	$W/m^2 \cdot K$
Nu	$0,023 \cdot Re^{0,8} \cdot Pr^{0,4}$	$0,0214 \cdot (Re^{0,8} - 100) Pr^{0,4}$	-
Re	$\frac{4 \cdot \dot{m}}{\pi \cdot D_{in,h} \cdot \mu}$	$\frac{4 \cdot \dot{m}}{\pi \cdot (D_{in,c} - D_{in,h}) \cdot \mu}$	-

Power each segment (x) and total power TEG (W_{TEG}) shown in Equations 22 and 23 (He et al., 2016).

$$\dot{w} = \dot{Q}_h - \dot{Q}_L \quad (22)$$

$$W_{TEG} = \sum_{n_x} w(x) \quad (23)$$

Pressure drop that occurs along the channel is caused by the friction factor of the fluid with the cross-section to be calculated by Equations 24 and 25.

$$\Delta p = 4F \left(\frac{L}{D_{in,h}} \right) \cdot \left(\frac{v^2 \cdot \rho}{2} \right) \quad (24)$$

$$F = \frac{0,0791}{Re^{0,25}} \quad (25)$$

RESULTS AND DISCUSSIONS

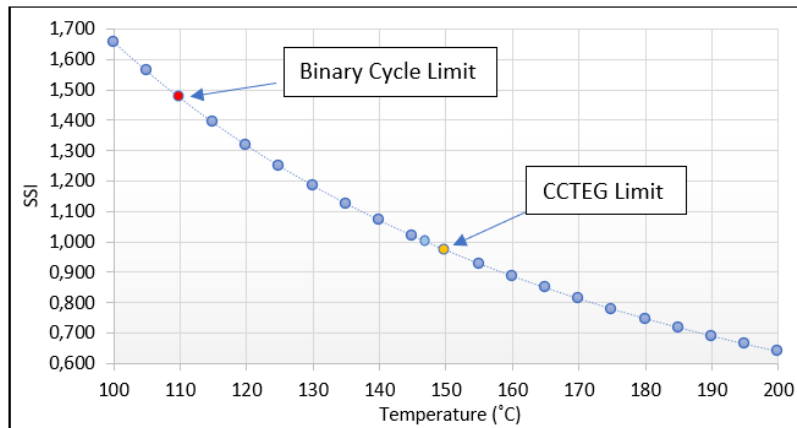


Figure 5. Comparison of operation limit temperature with SSI

Based on the results of silica deposition analysis with SSI parameters shown in Figure 5, it is explained that the utilization of brine with CCTEG has a maximum temperature limit of 150°C higher than the utilization limit for the binary cycle of 110 °C. This is considered a safety factor until it is reinjected back into the earth so that silica deposition does not occur along the surface of the pipe to the reinjection well. Potential of brine that can be used from 174°C to 150°C is shown in Table 5.

Table 5. Brine potential energy

Parameter	Value	Unit
\dot{m}	763.73	Kg/s
P	0.869	Mpa
T	174	°C
T_{min}	150	°C
E_n	79760	kW

The characteristics of saturated liquid brine fluid have an energy utilization potential of 79760 kW to be utilized by CCTEG before reaching the minimum reinjection temperature limit of 150°C which causes silica precipitation. The design of CCTEG is limited to a coldwater outlet temperature of

40°C so that it can be used for utility systems in the surrounding area. Specification of CCTEG design results is shown Table 6.

Parameter	Value	Unit
$\Delta T_{h,x}$	0,00254	°C
$\Delta T_{c,x}$	0,00069	°C
ZT_M	0,994	
Re_h	6820734	
Nu_h	6800	
Re_c	3872266	
Nu_c	8127	
$\Delta P(\text{hot side})$	173	kPa
$\Delta P(\text{cold side})$	1869	kPa
n_x	4713	
l_{CCTEG}	32	m
Voltage	51.2	kV
Current	10.5	A
Power	538,25	kW

CCTEG modeling simulation results are shown in Figure 6.

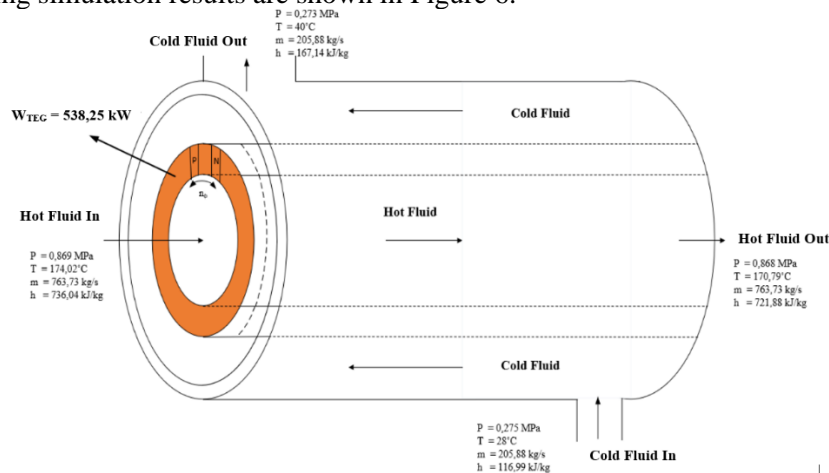


Figure 6. Simulation result of modelling CCTEG

The analyzed thermal system is a highly efficient heat exchanger with an effectiveness of approximately 95.5%. The hot fluid, with a mass flow rate of 763.73 kg/s and an inlet temperature of 174.02°C, releases 10,814 kW of energy, indicated by an enthalpy drop of 14.16 kJ/kg and a temperature decrease of 3.23°C. Meanwhile, the cold fluid, with a flow rate of 205.88 kg/s and an inlet temperature of 28°C, absorbs 10,325 kW of energy, experiencing an enthalpy increase of 50.15 kJ/kg and a temperature rise of 12°C. The power difference of 489 kW closely matches the transferred work (W_{TEG}) of 538.25 kW, suggesting minor external work or energy losses. With relatively small pressure changes in both fluids, the system demonstrates effective heat transfer performance.

The design of CCTEG was calculated using Microsoft Excel software with the electrical circuit of each TEG semiconductor component arranged in series. Heat transfer analysis in CCTEG on the hot and cold sides with a counter-flow model produces turbulent flow along the TEG. The pressure drop along the CCTEG was insignificant on both sides of the 173 kPa on the hot side and 1869 kPa on the cold side. The CCTEG power produced is 538.25 kW with a total of 2309370 TEG semiconductors distributed in 4719 segments. Energy potential utilization of 0.6% of the total available brine thermal energy.

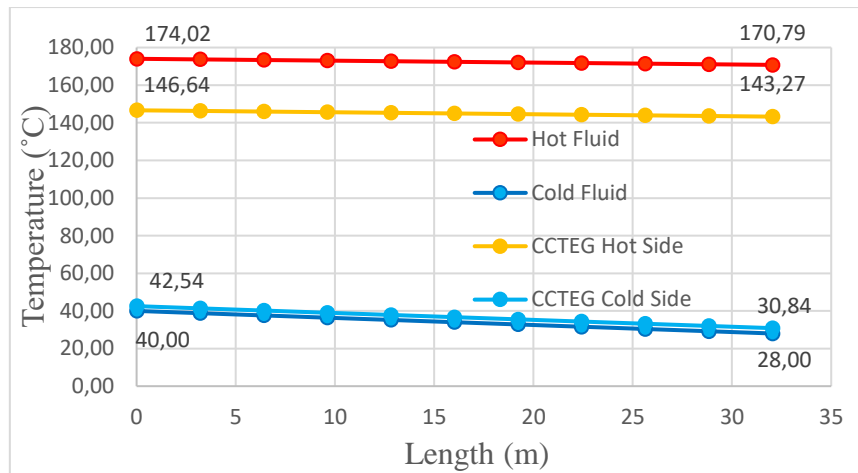


Figure 7. Temperature distribution on CCTEG

Based on Figure 7 temperature distribution on CCTEG use a counterflow heat exchanger system with four distinct thermal profiles. The hot fluid shows a moderate temperature drop from 174.02°C to 170.79°C, while the cold fluid exhibits a 12°C temperature rise from 28°C to 40°C, indicating efficient heat transfer. The CCTEG components display steeper temperature gradients, with the hot side cooling from 146.64°C to 143.27°C and the cold side heating from 30.84°C to 42.54°C, suggesting their role as thermoelectric generators or localized high-heat-flux zones. The near-parallel temperature curves of the primary fluids maintain a consistent 130°C temperature difference, characteristic of an effective counterflow arrangement, though the hot fluid's minimal temperature change (3.23°C) compared to the cold fluid implies a significantly higher heat capacity rate, likely due to its substantial mass flow rate (763.73 kg/s). The system demonstrates proper thermal isolation between streams, with no temperature crossover, while the CCTEG's distinct profile indicates additional energy extraction, warranting further investigation to optimize its integration within the heat exchanger system.

Analysis of the temperature distribution in the CCTEG along 32 meters shows that the brine exits the CCTEG by 170.79°C. The temperature difference on the hot and cold sides of the CCTEG with each fluid tends to be stable so that it produces maximum power in each TEG semiconductor with a significant temperature difference. On the hot fluid side, the temperature of the brine outlet is still greater than the silica deposition threshold of 150°C so that the brine does not allow silica scaling. On the cooling water side out of the CCTEG, the temperature is limited to 40°C and is flowed into the cooling pond to be used as a utility system in the surrounding area.

CONCLUSION

Based on the results of the CCTEG design in the Ulubelu Geothermal field, the following important things are obtained. Based on SSI reference the utilization of brine potential up to a temperature of 150°C. The results of the CCTEG design simulation require a TEG semiconductor 2309370 with Bismuth Telluride material modeled in a double pipe heat exchanger with a total length of 32 meters to produce 538.25 kW. The total utilization of brine energy potential is 0.6% of 79760 kW. An economic feasibility analysis needs to be carried out to compare the feasibility of technical and economic studies for actual implementation.

NOMENCLATURE

h	: Enthalpy (kJ/kg)
P	: Pressure (MPa)
Δp	: Pressure drop (kPa)
ΔT	: Temperature difference (°C)
S_{sat}	: Kondisi saturasi silika (m ²)
A	: Koefisien Seebeck (μV/K)
β	: Electric Resistivity (Ω.m)
λ	: Thermal Conductivity (W/m.K)

T	: Temperature (°C)
T_{min}	: Limit of minimum temperature (°C)
F	: Friction Factor
\dot{m}	: Mass flow (kg/s)
E_n	: Energy (kW)
$D_{out,h}$: Outer Diameter hot side (m)
$D_{in,h}$: Inner Diameter hot side (m)
$D_{out,c}$: Outer Diameter cold side (m)
$D_{in,c}$: Inner Diameter cold side (m)
n_ϕ	: Number of TEG semiconductor on segment
n_x	: Number of segment
Δ_x	: Gap of segments
\dot{Q}_f	: Heat released from brine to TEG segment
\dot{Q}_h	: Heat absorbed on the hot side
\dot{Q}_L	: Heat absorbed on the cold side
\dot{Q}_c	: Heat released from TEG segment to water condensate.

REFERENCES

- Al-Hababeh, O. M., Mohammad, A., Al-khalidi, A., Khanfer, M., & Obeid, M. (2018). Design optimization of a large-scale thermoelectric generator. *Journal of King Saud University - Engineering Sciences*, 30(2), 177–182. <https://doi.org/10.1016/j.jksues.2016.01.007>
- Bauknecht, A., Steinert, T., Spengler, C., & Suck, G. (2013). Analysis of Annular Thermoelectric Couples with Nonuniform Temperature Distribution by Means of 3-D Multiphysics Simulation. *Journal of Electronic Materials*, 42(7), 1641–1646. <https://doi.org/10.1007/s11664-012-2360-7>
- Darmawi, & Malau, R. H. (2018). Geothermal Energy Utilization and Environment Impact Prevention on Single Flash Steam Cycle System Case Study: PLTP Ulubelu - Lampung. *International Journal of Science and Research (IJSR)*, 7(7), 120–124.
- Ding, L. C., Singh, B. S. B., Remeli, M. F., Date, A. S., Singh, R., & Akbarzadeh, A. (2015). Prospects of power generation from geothermal energy using thermoelectric modules. *Proceedings World Geothermal Congress 2015*, 1–8.
- Ding, T., Liu, J., Shi, K., Hu, S., & Yang, H. (2020). Theoretical Study On Geothermal Power Generation Using Thermoelectric Technology: A Potential Way To Develop geothermal energy. *International Journal of Green Energy*, 18, 1–11. <https://doi.org/10.1080/15435075.2020.1854271>
- DiPippo, R. (1985). *Silica problem in the design of geothermal power plants*. <https://doi.org/10.2172/6067617>
- DiPippo, R. (2015). *Geothermal Power Plants: Principle, Applications, Case Studies And Enviromental Impact (4th ed)*. Butterworth-Heinemann.
- He, W., Guo, R., Liu, S., Zhu, K., & Wang, S. (2020). Temperature gradient characteristics and effect on optimal thermoelectric performance in exhaust power-generation systems. *Applied Energy*, 261, 114366. <https://doi.org/10.1016/J.APENERGY.2019.114366>
- He, W., Wang, S., Zhao, Y., & Li, Y. (2016). Effects of heat transfer characteristics between fluid channels and thermoelectric modules on optimal thermoelectric performance. *Energy Conversion and Management*, 113, 201–208. <https://doi.org/10.1016/J.ENCONMAN.2016.01.059>
- International Energy Agency. (2024). *Global electricity demand set to rise strongly this year*

and next, reflecting its expanding role in energy systems around the world.

- International Renewable Energy Agency. (2023). *World Energy Transitions Outlook 2023, Volume 1*.
- Li, K., Garrison, G., Zhu, Y., Horne, R., & Petty, S. (2021). Cost Estimation of Thermoelectric Generators. *46th Workshop on Geothermal Reservoir Engineering*, 1–8.
- Madruca, S. (2021). Modeling of enhanced micro-energy harvesting of thermal ambient fluctuations with metallic foams embedded in Phase Change Materials. *Renewable Energy*, 168, 424–437. <https://doi.org/10.1016/J.RENENE.2020.12.041>
- Muchtar, A., Tambunan, A. H., Machfud, & Novianto, A. (2018). Preliminary analysis of single-flash geothermal power plant by using exergy method: A case study from Ulubelu geothermal power plant in Indonesia. *International Journal of Renewable Energy Research*, 8(3). <https://doi.org/10.20508/ijrer.v8i3.8105.g7470>
- Yang, W., Zhu, W. C., Li, Y., Zhang, L., Zhao, B., Xie, C., Yan, Y., & Huang, L. (2022). Annular thermoelectric generator performance optimization analysis based on concentric annular heat exchanger. *Energy*, 239, 122127. <https://doi.org/10.1016/J.ENERGY.2021.122127>
- Zoui, M. A., Bentouba, S., Velauthapillai, D., Zioui, N., & Bourouis, M. (2022). Design and characterization of a novel finned tubular thermoelectric generator for waste heat recovery. *Energy*, 253, 124083. <https://doi.org/10.1016/J.ENERGY.2022.124083>